

# Protein adsorption and monocyte activation on germanium nanopyramids

Marco Riedel<sup>1</sup>, Bert Müller\*, Erich Wintermantel

*Department of Materials, ETH Zürich, Wagistrasse 23, CH-8952 Schlieren, Switzerland*

Received 14 June 2000; received in revised form 28 December 2000; accepted 11 January 2001

## Abstract

Germanium can form defect-free pyramidal islands on Si(1 0 0)- $2 \times 1$  with a height of 15 nm and a width of 60 nm. Using chemical vapor deposition we have prepared substrates with different nanopyramid densities to study the impact on contact angles, protein adsorption and cell behavior. The advancing contact angle of a water droplet of millimeter size significantly raises with nanopyramid density. The dynamic contact angle measurements reveal that the substrate surface is highly hydrophilic. On such a surface the adsorption of hydrophilic proteins, i.e. albumin and globulin, is drastically increased by the presence of nanopyramids. More important, however, the globulin is inactive after adsorption on nanopyramid edges. This observation is supported by the cytokine release of IL-1 $\beta$  and TNF- $\alpha$  of monocyte-like cell line U937. Consequently, the presence of nanopyramidal structures gives rise to less inflammatory reactions. © 2001 Elsevier Science Ltd. All rights reserved.

*Keywords:* Nanostructure; Germanium; AFM; Contact angle; Protein activity; Monocytes

## 1. Introduction

With the advent of nanostructured materials with extensions of less than 100 nm it is recognized that surface architecture may have a greater effect on cell behavior than chemical pattern [1]. It has become clear that the cell-substrate interactions, which have importance for use in cellular engineering and tissue repair, not only occur on the micrometer scale [2–4] but also on the nanometer scale [5,6]. However, cell experiments on substrates with a well-defined topography on atomic scale are rather scarce, because their preparation is usually complicated and based on highly sophisticated techniques. Furthermore, the characterization of surface morphology even by scanning probe techniques is ambiguous since surface roughness depends on the considered length scale. For example, the Wenzel ratio [7], i.e. the ratio between the actual surface and the projected one, that plays an important role in contact angle measurements, cannot be detected exactly [8]. To master these problems, we have prepared atomically flat substrates

with different densities of well-defined epitaxial islands (nanopyramids). These substrates, where the Wenzel ratio can be determined, are used to perform contact angle measurements, adsorption of selected proteins and in vitro assays with monocyte-like cells.

The preparation of silicon with atomically flat terraces of micrometer size is well known from semiconductor research and microelectronics industry, where generally the Si(00 1) surface is used [9–13]. The growth of germanium, which has a 4% larger lattice constant than silicon, on such a substrate has been described by layer plus island mode. The wetting layer, a uniformly strained germanium film, grows pseudomorphically to a thickness of 2–3 monolayers, followed by the formation of three-dimensional islands on top of the uniform film [11,14]. These islands have a pyramidal or prism-like shape and are free of dislocations [14]. At lower coverage the nanopyramids are square or elongated huts with {1 0 5} facets implying angles of 11.3° with the flat substrate [11]. Scanning tunneling microscopy images in Fig. 1 represent such pyramids. These hut clusters are about 6 nm high and 60 nm wide. Their formation on atomic scale is made visible using high-temperature scanning tunneling microscopy [15]. At higher coverages, the shape changes, and nanopyramids, termed dome cluster, are formed [14,16–18]. Here, the side planes are {1 1 3}

\* Corresponding author. Tel.: + 41-1-6336190; fax: + 41-1-6331120.

E-mail address: mueller@biocomp.mat.ethz.ch (B. Müller).

<sup>1</sup> Present address: ProBioGen AG, Berlin, Germany.

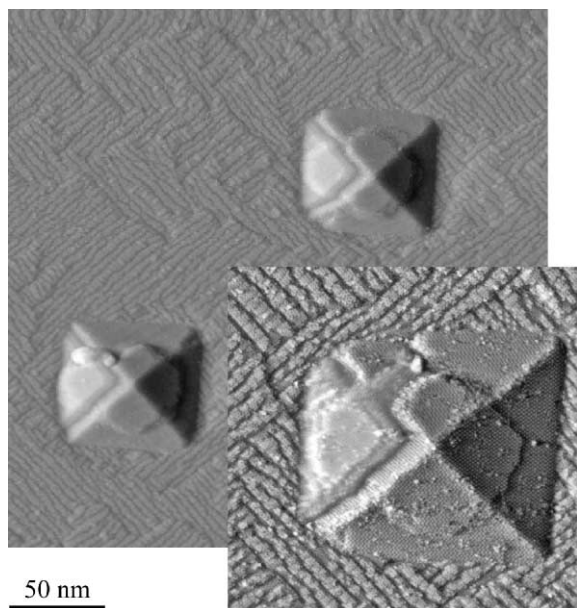


Fig. 1. Scanning tunneling microscopy images of germanium nanopylramids (hut clusters) grown on Si(001)- $2 \times 1$  at a substrate temperature of 550°C with a deposition rate of 0.16 monolayers/s by molecular beam epitaxy (germanium coverage 5.8 monolayers). The pyramids have a height of about 6 nm and a basis 60 nm  $\times$  60 nm and exhibit well-defined  $\{105\}$  facets. The atomic structure is visible in the inset, where the magnification is further increased by a factor of two. The facet on the left is not well resolved due to the imperfect STM tip.

and  $\{102\}$  facets, which gives rise to angles of 25.2° and 26.6°, respectively. Their basis is comparable with that of hut clusters but their height exceeds by more than a factor of two. More important, the Wenzel ratio, that is for pyramids basically  $1/\cos(\alpha)$ , where  $\alpha$  denotes the angle between facet and substrate, is larger by a factor of six for the dome clusters than for the hut clusters with respect to the flat surface. Therefore, our experiments, given in the present communication, are performed on substrates covered by dome clusters.

Compared to cells the nanopylramids are small and their effect on cell behavior is expected to be limited. Proteins such as bovine serum albumin (BSA) and bovine  $\gamma$ -globulin (BGG), on the other hand, have comparable sizes as shown in Table 1. The pyramid edges offer different adsorption sites. Consequently, one may assume that the nanopylramid density modifies protein adsorption and activity, since the adsorption site geometry can alter the conformation and thereby, the biological activity [19,20]. Such modifications in the protein adsorption and activity may improve the cell behavior. Here, we focus on the inflammatory reactions applying the monocyte-like cell line U937. Monocytes and especially the cells of U937 contain a special receptor ( $Fc\gamma$ RIIR), which allows interactions with the intact Fc fragment of BGG as present in bovine serum. These interactions result in activation characterized by the expression of the

Table 1

Sizes of Ge pyramids grown on Si(001) and specific proteins: BSA and BGG

Structural element	Area of base (nm <sup>2</sup> )	Height (nm)	Facets	Slope
Hut cluster [17]	60 $\times$ 60	6	$\{105\}$	10.9°
Dome cluster [17]	60 $\times$ 60	15	$\{113\}, \{102\}$	25.2°, 26.6°
BSA [28]	3.8 $\times$ 3.8	14.0		
BGG [28]	4.4 $\times$ 4.4	23.5		

cytokines interleukin-1 $\beta$  (IL-1 $\beta$ ) and tumor necrosis factor (TNF- $\alpha$ ) [21,22].

It should be noted that (oxidized) germanium alone is not cytotoxic [23–25] and, therefore, suitable for this study.

## 2. Experimental

### 2.1. Materials and chemicals

Bovine serum albumin labeled with fluorescein isothiocyanate (BSA, Lot 29F9318, 11.2 mol FITC mol<sup>-1</sup> BSA) and Tween® 20 (Lot 15H09293) were purchased from Sigma (St. Louis, USA). Furthermore, a fluorescein conjugated ChromPure bovine IgG, whole molecule (BGG, Lot 35829, 2.9 mol FITC mol<sup>-1</sup> BGG) from Jackson ImmunoResearch Lab. Inc. was used. This BGG was purified over affinity chromatography with immobilized anti-BGG-POD (see below) onto NHS activated Sepharose® (Pharmacia, Sweden) to get BGG molecules with very high biological activity. Horseradish peroxidase-conjugated goat anti-bovine IgG(H + L) (anti-BGG-POD, Lot A384-N394J) was from Southern Biotech Ass. Inc. As blocking reagent in globulin ELISA human serum albumin (20%, Lot 101911) from Behringwerke AG (Marburg, Germany) was used. For globulin ELISA a substrate consisted of 1% TMB (98 + %, Lot 45788/113797) and 0.01% H<sub>2</sub>O<sub>2</sub> in a sodium acetate buffer (0.2 M, pH = 6.0), all from Fluka, were used. Fetal calf serum (FCS, Lot 30F9267A, with 150  $\mu$ g/ml  $\gamma$ -globulin) and cell culture medium RPMI-1640 without glutamine were received from GibcoBRL.

### 2.2. Substrate preparation

Silicon wafers Si(001) 4 in. in diameter were purchased from Sico Meiningen Wafer GmbH, Germany. Germanium nanopylramids were epitaxially grown by chemical vapor deposition (CVD). The substrate temperature was varied between 520°C and 600°C, and the german pressure was between  $6 \times 10^{-5}$  and  $4 \times 10^{-4}$  mbar. The exact growth conditions are given in the figure captions. Substrates were processed under particle free atmosphere.

X-ray photoelectron spectroscopy measurements have proven that the substrates with the different pyramid densities are chemically equivalent [26].

### 2.3. Microscopy

Atomic force microscopy (AFM) measurements were performed using AUTOPROBE CP (Park Scientific Instruments, 1171 Borregas Avenue, Sunnyvale, California 94089).

For scanning electron microscopy (SEM) cells on the substrates were fixed by 3-day incubation in 3% glutaraldehyde. Subsequently, the solvent was stepwise exchanged (water by ethanol and ethanol by hexamethyl disilazane). These substrates were platinum coated by sputtering (sputter coater SCD004, Balzers). SEM images were recorded by the use of an S-2500C microscope (voltage = 15 kV, HITACHI, Japan) with an angle of view of 45°.

### 2.4. Contact angle measurement

The contact angles were determined with the system G2 (Kruess, Germany). The increase and decrease of the drop volume of ultra pure water on the substrate gives rise to the dynamic contact angle measurements of the advancing and the receding contact angles. After rinsing of substrates with ultra pure water for 2 h, the drop volume was increased or decreased in ten steps. Both the angles on the left and on the right were detected. Using 6 drops, 120 advancing and 120 receding contact angles were recorded and used for statistical analysis.

### 2.5. Protein adsorption

The adsorption experiments were made with FITC labeled BSA and BGG using a concentration of 100 µg/ml in phosphate buffered saline (PBS, pH = 7.4). Substrates were placed in 6-well cell culture plates. The accessible substrate area was fixed to 0.95 cm<sup>2</sup> using a special holder leaving only the active surface open to solution. After protein adsorption of 1 h, the substrates were rinsed with PBS and water. The adsorbed proteins were quantitatively eluted with 1.0 ml 0.2 N NaOH for 2 h. In addition, at this basic pH the FITC molecule is stable and has the highest fluorescent quantum yield. Without any additional manipulations, elutes were transferred to 24-well cell culture plates (Costar) and the fluorescence was measured with a fluorescence multi-well plate reader CytoFluor II (PerSeptive Biosystems). The excitation and emission wavelengths were set to 488/20 and 530/30 nm, respectively. Fluorescence was detected at four different gains and separately analyzed. At identical conditions the calibration was performed with 0.01, 0.025, 0.06, 0.15, 0.4 and 1.0 µg/ml BSA and BGG, respectively. The data are well fitted by second order regression.

### 2.6. Protein assays

In the present communication, protein activity is understood as the capability of recognition and, consequently, of affinity interactions between BGG and polyclonal anti-BGG-POD. Each anti-BGG-POD can recognize four binding sites in a BGG molecule. Because of steric reasons, interactions between one BGG and four anti-BGG-POD molecules are rather unlikely. For evaluation, an ELISA-like set-up was used. BGG protein adsorption was carried out as described above. After adsorption, the substrates were rinsed with PBS twice and blocked with a 2% HSA solution for 1 h. Substrates were rinsed with PBS and incubated with anti-BGG-POD in 2% HSA for an additional hour. For washing, PBS with 0.1% Tween was used. For each substrate 1.0 ml TMB (peroxidase substrate) was added and stopped with 0.1 ml 2 M H<sub>2</sub>SO<sub>4</sub> after 3 min. An amount of 0.2 ml of this solution was transferred to a 96-well plate and the absorbance was measured with ELISA reader Spectra Rainbow (SLT Lab Instruments, Austria) at a wavelength of 450 nm. Calibration was performed with 1, 3, 10, 30, 100 and 300 ng/ml anti-BGG-POD. The resulted curve is perfectly described by a Langmuir fit.

For cytokine ELISA 100 µl cell-free supernatant was diluted with 500 µl PBS. Three tests with 200 µl were performed. Cytokine ELISA (human TNF-α ELISA ultra sensitive and Quantikin™ human IL-1β, both from R&D Systems Inc., Minneapolis) were performed according to the instructions. Each value has a relative error of ±10%.

### 2.7. Cell culture

The monocyte-like cell line U937 (ATCC: CRL 1593) was cultivated in RPMI-1640 without glutamine with 5% FCS and 5% CO<sub>2</sub> at 37°C. The preliminary culture medium was totally changed every three days. The sterilized substrates of rectangular shape (about 1 cm<sup>2</sup>) were placed into the 24-well cell culture plate with a diameter of about 12 mm and incubated with 1 ml cell suspension with 3.6 × 10<sup>5</sup> cells/ml. After 5 days in culture, the cell number was determined, the cell suspension was centrifuged hard and the clear supernatant was stored at a temperature of -20°C before cytokine quantification. The cells were counted in an improved Neubauer chamber with Trypan blue.

## 3. Results

The substrate morphology is quantitatively characterized by atomic force microscopy. A selection of the AFM images is shown in Fig. 2. Although these images do not show the nanopylramids with atomic resolution, they give

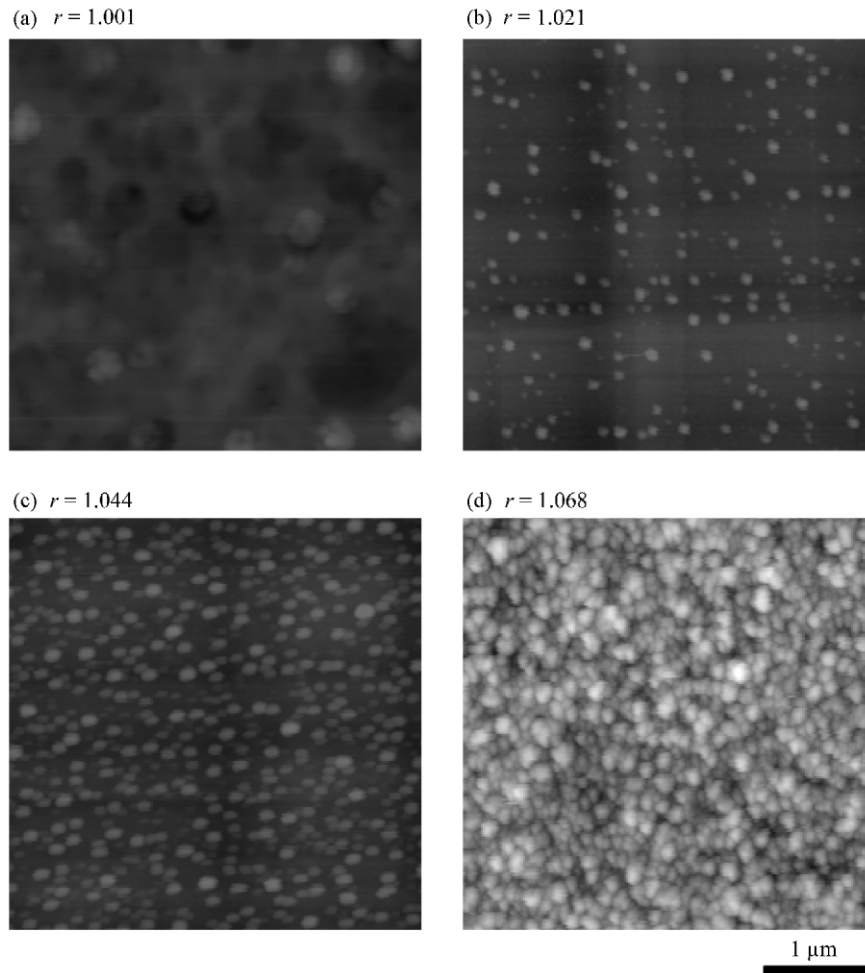


Fig. 2. AFM images illustrating the pyramid density. The roughness factor  $r$  corresponds to the ratio between the actual and geometric surface. The gray scale corresponds to 80 nm. The thin films were prepared under following conditions: (a) subsequent growth of  $4 \times 20$  ml/3 ml silan/german with 20 ml capping grown at a temperature of  $600^\circ\text{C}$  and a total pressure of  $3.3 \times 10^{-4}$  mbar, (b) mixture of 20 ml silan with 0, 3, 7, 13, 20, 30 ml german followed by 20 ml silan and 20 ml german grown at a temperature of  $550^\circ\text{C}$  and a total pressure of  $1.3 \times 10^{-4}$  mbar, (c) 60 ml silan, mixture of 20 ml silan with 40 ml german, 40 ml silan, 20 ml german grown at a temperature of  $520^\circ\text{C}$  and a total pressure of  $6.7 \times 10^{-5}$  mbar, (d) 20 ml silan with 0, 3, 8, 15, 22, 0, 30, 0 ml german followed by 20 ml german grown at a temperature of  $600^\circ\text{C}$  and a total pressure of  $1.5 \times 10^{-4}$  mbar.

an idea of the surface roughness and can be used to determine the pyramid density. The commercially available AFM programs directly yield the root mean square roughness ( $R_{\text{RMS}}$ ) and the mean roughness ( $R_{\text{AVE}}$ ) from the images. Both quantities are summarized in Table 2 for an image size of  $5 \mu\text{m} \times 5 \mu\text{m}$ . The values are reasonable estimates of the surface morphology. However, they crucially depend on scan size [27]. This dependence again relies on the roughness. Consequently, the quantities are inadequate to describe the pyramid density on the flat substrates and, therefore, the surface roughness, precisely.

The aim of the present study includes the determination of the roughness factor  $r$  (Wenzel ratio [7]). Therefore, we have extracted the actual surface using a commonly used computer code, but with the exception of very flat surfaces the program also delivered values,

which significantly change with scan size. Images with higher magnification result in larger values because more details are accessible. That means, the actual surface cannot be well reproduced by the AFM images of micrometer size and the available computer codes.

Finally, we have counted the pyramids on certain area at different images to determine the pyramid density with high precision. From the pyramid density it is straightforward to determine the actual surface because the mean pyramid height and pyramid shape are known. This treatment is corroborated by the height measurements, which give a constant value of  $(15 \pm 3)$  nm for the substrates used. Hence, it is possible to quantify the surface roughness factor with unequaled accuracy.

Because the roughness factor is quantified with appropriate accuracy, the relationship of contact angles on

roughness can be uncovered even if the differences between the substrates seem to be modest. The results, represented in Fig. 3, elucidate that the advancing contact angle of water can change by 20° from flat substrates to substrates with maximum pyramid density, whereby the receding contact angle remains constant within the error bars. Note the contact angle measurement is rather difficult for values below 15°. To reduce the error bars, we have carried out six independent measurements each on the bare silicon wafer (not shown), on the flat germanium wetting layer and on the four nanostructured substrates reproduced in Fig. 2. Each measurement consists of 20

angles at advancing and at receding water droplets. The related values for the contact angle hysteresis including the significance data are summarized in Table 3. It should be mentioned, that the contact angles have to be measured after water treatment to obtain a reproducible result since the angles measured before water treatment depend crucially on the ambient conditions, in particular on humidity.

Fig. 4 shows the adsorption of two selected proteins: FITC labeled albumin (BSA) and FITC labeled  $\gamma$ -globulin (BGG) on the substrates with different

Table 2  
Quantification of surface roughness by the use of AFM images

Substrate	a	b	c	d
$R_{RMS}$ (nm) <sup>a</sup>	3.4	4.2	4.9	10.8
$R_{AVE}$ (nm) <sup>a</sup>	2.6	3.1	3.8	8.6
Effective surface <sup>b</sup>	1.001	1.006	1.012	1.048
Cluster density ( $10^{-12} \text{ m}^{-2}$ )	0.8	13	26	40
Roughness factor $r$	1.001	1.021	1.044	1.068

<sup>a</sup>The root mean square roughness  $R_{RMS}$  and the mean roughness  $R_{AVE}$  are directly determined by the computer code ProScan Image Processing version 1.5.1 of Park Scientific Instruments.

<sup>b</sup>The effective surface, which should correspond to the roughness factor is calculated from images with a size of  $5 \mu\text{m} \times 5 \mu\text{m}$  by the computer code “Image SXM v1.62” (<http://reg/ssci.liv.ac.uk/>). It turns out, however, that these values depend on image size and resolution. Therefore, the surface roughness has been calculated on the basis of cluster counting and cluster geometry.

Table 3  
Cell numbers and cytokine concentrations after five-day cultivation of U937 cells on Ge nanopyramids

Substrate	Flat	a	b	c	d
<b>Contact angles</b>					
Hysteresis $\Delta\theta$ (deg)	27.3	31.7	32.9	34.3	38.5
Significance ( $n = 238, P < 0.01$ ) <sup>a</sup>	—	+; $t = 13.49$	+; $t = 5.10$	-; $t = 1.72$	+; $t = 9.41$
<b>BGG activity</b>					
anti-BGG A (ng/cm <sup>2</sup> )	19.96	19.27	23.23	20.91	13.09
SD <sup>b</sup> ( $n = 4$ ) (ng/cm <sup>2</sup> )	1.50	0.74	1.74	1.24	1.18
Significance ( $n = 6, P < 0.01$ ) <sup>a</sup>	—	-; $t = 0.82$	+; $t = 4.17$	-; $t = 2.16$	+; $t = 9.18$
<b>Cell culture<sup>c</sup></b>					
Viable cells ( $10^5$ c/ml)	7.84	0	2.22	3.36	10.92
SD <sup>b</sup> ( $n = 8$ ) ( $10^5$ c/ml)	0.88	0	0.35	1.31	1.50
Viability (%)	58	0	13	20	77
IL-1 $\beta$ (pg/ml)	27.8	204.9	54.1	50.0	27.6
IL-1ra (pg/ml)	8112	7869	8308	9030	8142
TNF- $\alpha$ (pg/ml)	16.6	20.4	16.0	17.9	14.7
IL-1 $\beta$ /IL-1ra ( $\times 0.001$ )	3.43	26.04	6.51	5.53	3.39

<sup>a</sup>Significance test from substrate to substrate: from flat to a, from a to b etc.

<sup>b</sup>SD is the standard deviation.

<sup>c</sup>The inoculum was  $(3.66 \pm 0.78) \times 10^5$  cells per ml with a viability of 88 %. The measured cytokine concentrations for IL-1 $\beta$ , IL-1ra and TNF- $\alpha$  were 13.8, 7806, and 16.5 pg/ml, respectively.

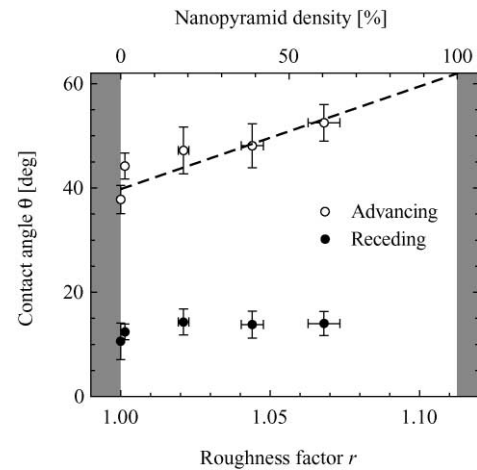


Fig. 3. Contact angles of water vs. roughness factor to elucidate the increase of the contact angle hysteresis with the nanometer scale surface roughness. The measurements were performed at room temperature. The dashed line represents the linear regression of advancing angles.

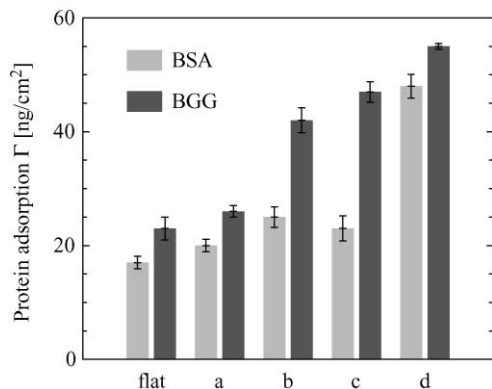


Fig. 4. Protein adsorption of BSA and BGG onto surfaces with different nanopyramid density. Flat denotes a substrate where a flat germanium film 2–3 monolayers thick has been grown on Si(001) but no pyramids are formed yet. The other indices are related to Fig. 2.

nanopyramid density. The total amount of proteins is well below monolayer coverage. The presence of nanopyramids has an immense effect on the adsorption of BSA as well as BGG. On the flat germanium substrate,  $(23 \pm 2)$  ng/cm<sup>2</sup> of BGG were adsorbed. Assuming a molecular weight of 160 kD for BGG [28], this amount corresponds to  $(860 \pm 80)$  BGG molecules/μm<sup>2</sup>. By an increase of the effective surface by 7%, the adsorbed proteins raise by a factor of 2.5. That means, the adsorption sites are different on the flat and the pyramidal surface. Nanopyramids appear to provide much more effective adsorption sites.

Because of the stronger protein-substrate binding on the nanostructured surfaces the activity of the proteins could be modified. Indeed, the amount of biologically active BGG does not scale with the adsorbed BGG as shown in Table 3. The amount of adsorbed anti-BGG is even lowered on the substrate with a high nanopyramid density. This finding is supported by cell viability and cytokine release of monocyte-like cell-line-U937 cells. The cells were stained with Trypan blue to distinguish between viable cells and dead cells. High pyramid densities result in an increased number of viable cells. At highest nanopyramid densities the viability determined by Trypan blue reached a value of 77% (cp. Table 3). The cells on the substrate with lowest nanopyramid density were found to be Trypan blue colored without exception. The penetration of Trypan blue into the cells via its membrane is characteristic for dead cells or massively damaged cells.

#### 4. Discussion

Epitaxial growth (molecular beam epitaxy or chemical vapor deposition) offers the formation of nanostructures under well-defined conditions in a natural way. By the

choice of the growth conditions the surface morphology including island density, island size and island size distribution can be tailored [29]. On the other hand, there are thermodynamic constraints, which limit the variations. For the present system Ge/Si(001), the island density can be easily varied by the substrate temperature and the coverage. Size and shape of the three-dimensional islands are almost independent in a wide range of growth conditions since the islands must have a certain size to become stable [30]. The size distribution can be even improved by self-organization in the growth of multilayer sandwich structures [31–33]. The size of the islands can be reduced by carbon pre-deposition [34,35]. Here, the pyramids change their shape also and become flat on top. On the other hand, the pyramid size can be increased by annealing [36–39]. This process is related to a partial alloying between germanium and silicon. Consequently, epitaxial growth gives rise to a great variety of nanostructures that can serve as ideal templates for fundamental studies of the interactions between cells and nanometer scale structures.

Substrates with topological features on nanometer level can alter the physical properties of the surfaces. Hydrophobicity belongs to these properties and plays an important role in biocompatibility [40–42]. To distinguish between hydrophilic and hydrophobic surfaces, the Young's angle of water is used. This equilibrium angle is smaller than 90° for hydrophilic and larger than 90° for hydrophobic surfaces. Using dynamic contact angle measurements, the Young's angle  $\theta_e$  is found by the intersection of the fits for advancing and receding angles vs. contact angle hysteresis  $\Delta\theta$  with the ordinate at  $\Delta\theta = 0$  [8], as shown in Fig. 5. The contact angle hysteresis is defined by  $\Delta\theta = \theta_a - \theta_r$ . As a result, one finds a system of two linear equations:

$$\theta_a = A_a \Delta\theta + \theta_e$$

$$\theta_r = A_r \Delta\theta + \theta_e$$

with  $A_a = A_r + 1$ . The Young's equilibrium contact angle is found to be close to zero associated with the water pre-treatment. The inaccessible regions of Fig. 5 are gray-colored to illustrate the relatively small window of contact angle hysteresis available by dome cluster nanostructuring. The dynamic measurements give access not only to the equilibrium contact angle but also to the slope ( $A_a$  and  $A_r$ , respectively). It is attributed to the resistance of the water layer adsorbed to the nanostructured substrate to the wetting by water. This electronic effect is related to the dipolar character of the water molecules with the surface charges of the substrate resulting in a steering effect. Hence, dynamic contact angle measurements provide a mean to characterize the surface morphology and roughness, as we will describe elsewhere, in detail [43]. Note that the plot in Fig. 5 does not contain directly the surface roughness.

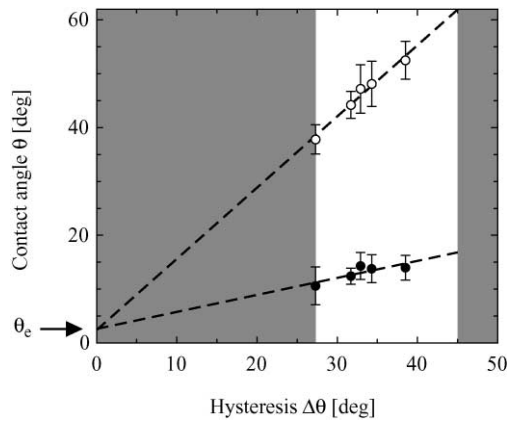


Fig. 5. Advancing (open cycles) and receding (filled cycles) contact angles vs. contact angle hysteresis for water on surfaces with different Ge nanopyramid density. The dashed lines are fitted by linear regression. The gray colored regions are not accessible by measurement. The Young's angle  $\theta_e$  derived is extremely small or even zero.

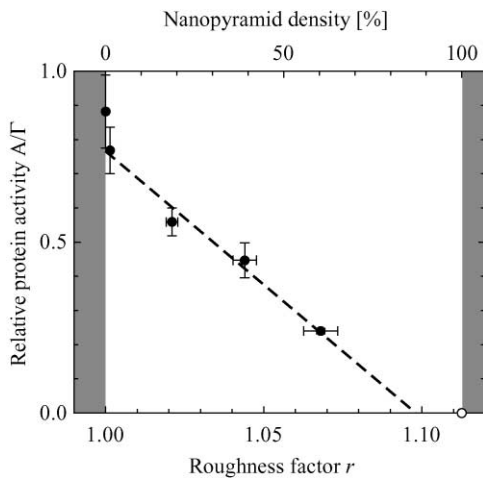


Fig. 6. Ratio between anti-BGG and BGG as a function of the roughness factor. The ratio decreases with pyramidal density as illustrated by a linear fit, reaching zero just below maximal possible pyramid density (open cycle).

The presence of the nanopyramids plays a crucial role in protein adsorption and activity. On flat substrates without pyramids the BGG is almost completely active, as demonstrated by the data of Fig. 4 and Table 3. On the substrates with nanopyramids, the amount of adsorbed protein is significantly increased. However, BGG is not active any more as shown in Fig. 6. The relative activity of BGG steadily decreases with nanopyramid density. The edges of the nanopyramids are assumed to be effective adsorption sites changing the conformation of the protein so that it becomes inactive. If the whole substrate is covered by nanopyramids, the adsorbed BGG is totally inactive (open circle in Fig. 6). This happens well below the maximal nanopyramid density, since BGG adsorption is obviously dominated by the nanopyramid edges.

Table 4  
Comparison of pyramid density and density of adsorbed proteins<sup>a</sup>

Substrate	a	b	c	d
Nanopyramid density (nanopyramids/ $\mu\text{m}^2$ )	0.84	12.56	26.08	40.16
BSA (molecules/ $\mu\text{m}^2$ )	1640	2060	1890	3950
BGG (molecules/ $\mu\text{m}^2$ )	980	1580	1760	2060

<sup>a</sup>For the determination of the protein density, the molecular weights given in ref. [28] are used: BSA 73 000 g/mol and BGG 160 000 g/mol.

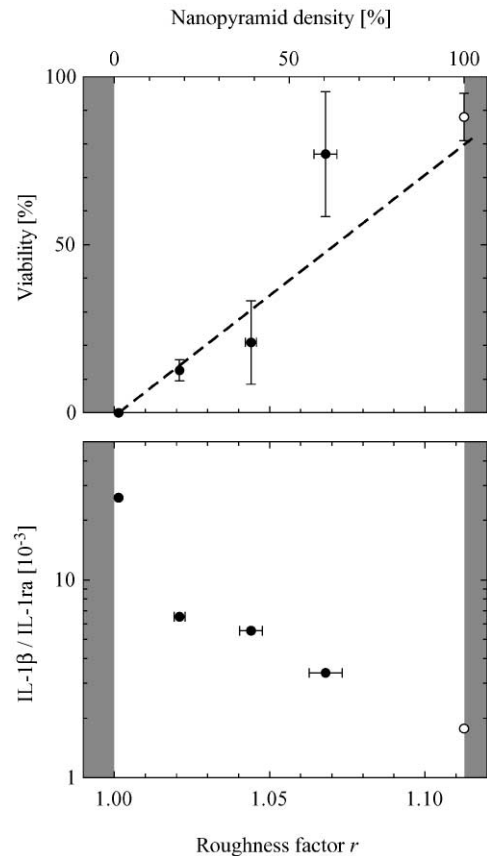


Fig. 7. Both the viability of monocyte-like cell line U937 and the ratio between the released proteins IL-1 $\beta$  and IL-1ra exhibit a strong correlation to pyramid density, reaching the reference at the maximal possible pyramid density (open cycles).

The densities of BSA, BGG, and anti-BGG-POD are compared with the nanopyramid density in Table 4. On the flat germanium wetting layer, we found a density of 1400 BSA molecules per  $\mu\text{m}^2$  and a density of 860 BGG molecules per  $\mu\text{m}^2$ . This density increases with the nanopyramid density, but not in a linear fashion. For the low nanopyramid densities, the number of additionally adsorbed proteins at the pyramids exceeds 100, whereas at the high nanopyramid densities, we found about 30 additionally adsorbed proteins per pyramid. Since the

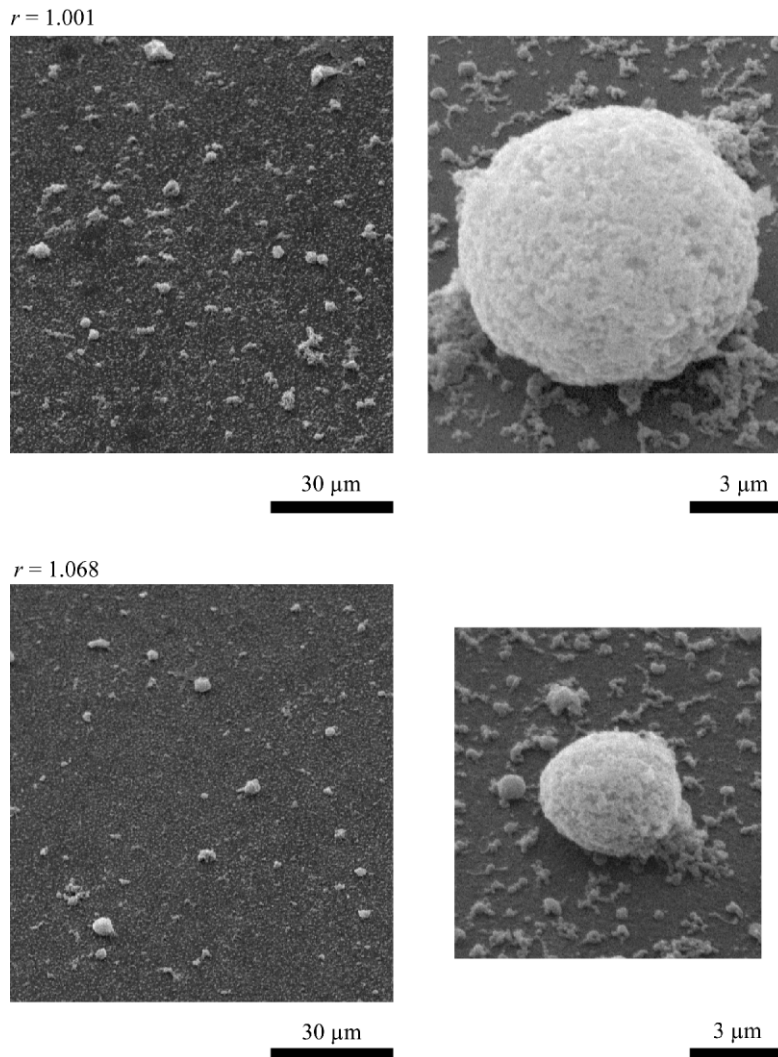


Fig. 8. SEM images of the plain (Fig. 2a) and rough (Fig. 2d) substrate with two magnifications. The substrate with few pyramids shows large amounts of cells and cell debris. Furthermore, the cells are a factor of two larger in diameter than on the surface with high pyramid density in agreement with cytokine release (cf. Table 3). Note a typical cell size corresponds to the sizes of the AFM images in Fig. 2.

number of additionally adsorbed proteins is so high, we conclude, that the nanopyramids not only provide special nucleation sites but also give rise to nucleation centers resulting in a certain degree of order of the proteins adsorbed at or near the pyramids.

The protein activity measurements are consistent with *in vitro* assays using monocytes. Their viability is zero on the substrate with only a very few nanopyramids and increases with the surface roughness until at maximal pyramid density where the viability reaches the reference value. The number of viable cells is a result of cell activation. During activation cytokines, i.e. IL-1 $\beta$  and TNF- $\alpha$ , are expressed. On one hand, the cytokine release leads to an amplified activation, and, on the other hand, TNF- $\alpha$  is cytotoxic for the monocyte-like cell line U937 [44]. Consequently, high activation means low viability. It is confirmed by the data given in Table 3, which show that the

expression of TNF- $\alpha$  is highest for the monocytes on the substrate with only a few nanopyramids and lowest for the substrate with the highest pyramid density. In addition, the results are also confirmed by the cytokine IL-1 $\beta$  release. The amount of IL-1 $\beta$ , one of the most crucial cytokines in inflammatory reactions decreases with pyramid density. More important for the inflammatory behavior is the ratio of the cytokine IL-1 $\beta$  and its receptor antagonist IL-1ra [45]. This ratio exhibits a more than exponential decay with the roughness factor, as verified by Fig. 7. This behavior is qualitatively supported by electron microscopy images of the cells and their fragments. Fig. 8 represents two images of the substrate with the lowest pyramid density and two images of that with the highest density on different scale showing an increased amount of cell fragments and more expanded cells.

## 5. Conclusions

Epitaxial growth of germanium on Si(001) can be used in a natural way to realize nanopylramids of almost identical size and shape with different density and without any use of lithographic techniques. Counting these nanopylramids, the actual surface and the roughness factor (Wenzel ratio) are determined with high precision. Since we have focused our study on dome clusters with facets, which form an angle of about 26° with the substrate, the roughness factor can be varied between 1.0000 and 1.1126. The nanopylramids give rise to a strong interaction between BSA and BGG, on one hand, and the substrate, on the other hand, changing the protein conformation. BGG adsorbed on the nanopylramids becomes inactive. Related experiments with monocyte-like cells reveal a strong correlation between nanopylramid density and cell viability as well as protein release responsible for inflammatory behavior. Along these lines, features on the nanometer scale such as nanopylramids can reduce the inflammatory reactions of various implants by application of structural compatibility.

## Acknowledgements

The authors are grateful to Oliver Leifeld for STM measurements and to Dietmar Heger and Detlev Grützmacher (Paul Scherrer Institute, Switzerland) for substrate preparation and related AFM measurements. The support of Rolf Hofer (ETH Zürich, Switzerland) during the extended contact angle measurements is appreciated. Finally, we acknowledge the critical reading of the manuscript by Jeffrey A. Hubbell (ETH Zürich).

## References

- [1] Curtis A, Wilkinson C. New depths in cell behaviour: reactions of cells to nanotopography. *Biochem Soc Symp* 1999;65:15–26.
- [2] Singhvi R, Kumar A, Lopez GP, Stephanopoulos GN, Wang DIC, Whitesides GM, Ingber DE. Engineering cell shape and function. *Science* 1994;264:696–8.
- [3] den Braber ET, de Ruijter JE, Smits HTJ, Ginsel LA, von Recum AF, Jansen JA. Quantitative analysis of cell proliferation and orientation on substrata with uniform parallel surface microgrooves. *Biomater* 1996;17:1093–9.
- [4] Chehroudi B, McDonnell D, Brunette DM. The effects of micro-machined surfaces on formation of bonelike tissue on subcutaneous implants as assessed by radiography and computer image processing. *J Biomed Mater Res* 1997;34:279–90.
- [5] Webster TJ, Siegel RW, Bizios R. Osteoblast adhesion on nanophase ceramics. *Biomater* 1999;20:1221–7.
- [6] Smith L, Nguyen T, Dennis JR, Hong J, Vogel V. Nanoscale topography influences fibroblast alignment and the architecture of cell-deposited extracellular matrix. 2001; in preparation.
- [7] Wenzel RN. Resistance of solid surfaces to wetting by water. *Ind Eng Chem* 1936;28:988–94.
- [8] Kamusewitz H, Possart W, Paul D. The relation between Young's equilibrium contact angle and the hysteresis on rough paraffin wax surfaces. *Coll Surf A* 1999;156:271–9.
- [9] Marée JM, Nakagawa K, Mulders FM, van der Veen JF, Kavanagh KL. Thin epitaxial Ge-Si(111) films: study and control of morphology. *Surf Sci* 1987;191:305–28.
- [10] Mo Y-W, Kariotis R, Swartzentruber BS, Webb MB, Lagally MG. Growth of Si on flat and vicinal Si(001) surfaces: a scanning tunneling microscopy study. *J Vac Sci Technol* 1990;8:232–6.
- [11] Mo YW, Savage DE, Schwarzentruer BS, Lagally MG. Kinetic Pathway in Stranski-Krastanov Growth of Ge on Si(001). *Phys Rev Lett* 1990;65:1020–3.
- [12] Mo YW, Kleiner J, Webb MB, Lagally MG. Activation energy for surface diffusion of Si on Si(001): a scanning-tunneling-microscopy study. *Phys Rev Lett* 1991;66:1998–2001.
- [13] Köhler U, Jusko O, Müller B, Hoegen MH-v, Pook M. Layer-by-layer growth of germanium on Si(100): strain-induced morphology and the influence of surfactants. *Ultramicroscopy* 1992;42–44:832–7.
- [14] Eaglesham DJ, Cerullo M. Dislocation-free Stranski-Krastanov growth of Ge on Si(100). *Phys Rev Lett* 1990;64:1943–6.
- [15] Kästner M, Voigtländer B. Kinetically self-limiting growth of Ge islands on Si(001). *Phys Rev Lett* 1999;82:2745–8.
- [16] Ross FM, Tersoff J, Tromp RM. Coarsening of self-assembled Ge quantum dots on Si(001). *Phys Rev Lett* 1998;80:984–7.
- [17] Medeiros-Ribeiro G, Bratkovski AM, Kamins TI, Ohlberg DAA, Williams RS. Shape transition of germanium nanocrystals on a silicon (001) surface from pyramids to domes. *Science* 1998; 279:353–5.
- [18] Ross FM, Tromp RM, Reuter MC. Transition states between pyramids and domes during Ge/Si island growth. *Science* 1999; 286:1931–4.
- [19] Wahlgren M, Arnebrant T. Protein adsorption to solid surfaces. *Trends Biotech* 1991;9:201–8.
- [20] Underwood PA, Steele JG, Dalton BA. Effects of polystyrene surface chemistry on the biological activity of solid phase fibronectin and vitronectin, analysed with monoclonal antibodies. *J Cell Sci* 1993;104:793–803.
- [21] Dinarello CA, In: Bomford R, Henderson B, editors. Was the original endogenous pyrogen interleukin-1? Amsterdam: Elsevier, 1989. p. 17–28.
- [22] Gearing A, Thorpe R, In: Bomford R, Henderson B, editors. Assay of interleukin-1. Amsterdam: Elsevier, 1989. p. 79–91.
- [23] Townsend JD, Hamilton AI, Sbordone L. Biologic evaluation of a silver-copper-germanium dental casting alloy and a gold-germanium coating alloy. *J Dent Res* 1983;62:899–903.
- [24] Han C, Wu G, Yin Y, Shen M. Inhibition by germanium oxide of the mutagenicity of cadmium chloride in various genotoxicity assays. *Food Chem Toxicol* 1992;30:521–4.
- [25] Lee CH, Lin RH, Liu SH, Lin-Shiau SY. Effects of germanium oxide and other chemical compounds on phenylmercury acetate-induced genotoxicity in cultured human lymphocytes. *Environ Mol Mutagen* 1998;31:157–62.
- [26] Müller B, Riedel M, Michel R, De Paul SM, Hofer R, Heger D, Grützmacher D. The impact of nanometer-scale roughness on contact-angle hysteresis and globulin adsorption. *J Vac Sci Technol* 2001; submitted.
- [27] Müller B. Natural formation of nanostructures: from fundamentals in metal heteroepitaxy to applications in optics and biomaterials science. *Surf Rev Lett* 2001;8.
- [28] Gölander CG, Kiss E. Protein adsorption on functionalized and ESCA-characterized polymer films studied by ellipsometry. *J Coll Interface Sci* 1988;121:240–53.
- [29] Venables JA, Spiller GDT, Hanbücken M. Nucleation and growth of thin films. *Rep Prog Phys* 1984;47:399–459.
- [30] Kamins TI, Carr EC, Williams RS, Rosner SJ. Deposition of three-dimensional Ge islands on Si(001) by chemical vapor

- deposition at atmospheric and reduced pressures. *J Appl Phys* 1997;81:211–9.
- [31] Tersoff J. Self-organization in growth of quantum dot superlattices. *Phys Rev Lett* 1996;76:1675–8.
- [32] Teichert C, Lagally MG, Peticolas LJ, Bean JC, Tersoff J. Stress-induced self-organization of nanoscale structures in SiGe/Si multilayer films. *Phys Rev B* 1996;53:16334–7.
- [33] Teichert C, Bean JC, Lagally MG. Self-organized nanostructures in  $\text{Si}_{1-x}\text{Ge}_x$  films on Si(001). *Appl Phys A* 1998;67:675–85.
- [34] Leifeld O, Grützmacher D, Müller B, Kern K. Ge-quantum dots on Si(001) tailored by carbon predeposition. *Mater Res Soc Proc* 1998;533:183–9.
- [35] Leifeld O, Müller E, Grützmacher D, Müller B, Kern K. In situ scanning tunneling microscopy study of C-induced Ge quantum dot formation on Si(100). *Appl Phys Lett* 1999;74:994–6.
- [36] Kamins TI, Williams RS. A model for size evolution of pyramidal Ge islands on Si(001) during annealing. *Surf Sci* 1998; 405:L580–6.
- [37] Medeiros-Ribeiro G, Kamins TI, Ohlberg DAA, Williams RS. Annealing of Ge nanocrystals on Si(001) at 550°C: metastability of huts and the stability of pyramids and domes. *Phys Rev B* 1998;58:3533–6.
- [38] Kamins TI, Medeiros-Ribeiro G, Ohlberg DAA, Williams RS. Dome-to-pyramid transition induced by alloying of Ge islands on Si(001). *Appl Phys A* 1998;67:727–30.
- [39] Kamins TI, Medeiros-Ribeiro G, Ohlberg DAA, Williams RS. Evolution of Ge islands on Si(001) during annealing. *J Appl Phys* 1999;85:1159–71.
- [40] Vienken J, Diamantoglou M, Hahn C, Kamusewitz H, Paul D. Considerations on developmental aspects of biocompatible dialysis membranes. *Artif Organs* 1995;19:398–406.
- [41] Lee JH, Lee JW, Khang G, Lee HB. Interaction of cells on chargeable functional group gradient surfaces. *Biomaterials* 1997; 18:351–8.
- [42] Knoell T, Safarik J, Cormack T, Riley R, Lin SW, Ridgway H. Biofouling potentials of microporous polysulfone membranes containing a sulfonated polyether-ethersulfone/polyether-sulfone block copolymer: correlation of membrane surface properties with bacterial attachment. *J Membr Sci* 1999; 157:117–38.
- [43] Riedel M, Müller B, Hofer R, Wintermantel E. in preparation.
- [44] Cairns JA, Guy GR, Tan YH. Interleukin-6 regulates the cytotoxic effect of tumour necrosis factor on U937 cells. *Immunology* 1992;75:669–73.
- [45] DeFife KM, Shive MS, Hagen KM, Clapper DL, Anderson JM. Effects of photochemically immobilized polymer coatings on protein adsorption, cell adhesion and the foreign body reaction to silicon rubber. *J Biomed Mater Res* 1999;44: 298–307.